Multiscale modeling of the dynamical conductivity of self-assembled nanoparticle networks: Numerical simulations vs analytical models

Louis Merle, Adrien Delpoux, Adnen Mlayah, J. Grisolia

Multiscale modeling of the dynamical conductivity of self-assembled nanoparticle networks: numerical simulations versus analytical models

L. Merle[1], A. Delpoux[1], A. Mlayah[2,3], J. Grisolia[*1]

[1] LPCNO, Université de Toulouse, INSA, CNRS, UPS, 135 Avenue de Rangueil, 31077 Toulouse, France,

[2] CEMES, Université de Toulouse, CEMES-CNRS, 29 rue Jeanne Marvig, 31055 Toulouse, France,

[3] LAAS, Université de Toulouse, CNRS, UPS, 7 Av. du Colonel Roche, 31400 Toulouse, France,

*Corresponding author: jeremie.grisolia@insa-toulouse.fr

Abstract:

Impedance spectroscopy experiments are able to reveal the fundamental charge transport properties of a wide variety of complex disordered and nano-structured materials providing that appropriate modeling tools are used. In this paper, we present a numerical simulation-based approach to model the dynamical conductivity of networks formed by self-assembled metal nanoparticles. The inter-particle nano-resistance and nano-capacitance are implemented at the nano-scale assuming inter-particle charge transfer and accumulation mechanisms which can be adapted depending on the nature of the nano-particles and of the surrounding medium. The actual positions and spatial arrangements of the nanoparticles within the network are taken into consideration, allowing the attributes of percolating conducting routes to be extracted, classified, and compared in terms of path conductance and statistical distribution of path lengths. Our findings are contrasted to those obtained using analytic models, which are commonly used but however rely on strong assumptions about the electric properties of the conducting paths. We address these assumptions and show that in the case of weakly disordered systems, there is a general agreement between numerical simulations and analytic modeling-based approaches. In the case of disordered networks where nano-particle size and position fluctuations are included, we show that the path length distribution is frequency dependent and can differ significantly from the log-normal distribution usually assumed in the analytic models. The impedance of individual pathways may be extracted from the numerical simulations; we discovered that the conductance and susceptance of a specific path are frequency-dependent and inversely proportional to the path length only in ordered networks. Strong scattering of conductance values is caused by disorder effects. The developed numerical approach is generic and applies to most nano-devices where charge transport relies on percolation; it allows to bridge the gap between the nano-scale and micro-scale electric characteristics and thus permits a deeper understanding of the charge transport properties of nano-structured materials.

Introduction:

The understanding of the unique properties of nanoparticles networks and their exploitation for the development of innovative functional devices is advancing rapidly. Indeed, many applications are based on the electronic, optic, or magnetic properties emerging from the multi-scale interaction between

nanoparticles in hierarchical assemblies [1–4]. Amorphous semiconductors, ionic conducting glasses, ceramics, ionic or electronic conducting polymers, metal cluster compounds, transition metal oxides… [5–7], have a common frequency-dependent conductivity $\sigma(\omega)$ that is characterized by a transition angular frequency ω_t from a low-frequency *DC* plateau to a dispersive high frequency *AC* region. $\sigma(\omega)$ can be approximated by an empirical power law $\sigma(\omega) = \sigma_{DC} + A\omega^n$, where *n* is a fractional exponent and *A* a pre-exponential constant, and has been dubbed the "universal power law" (UPL) by Jonscher et al. [8,9]. Several published works assume that the *n* exponent is a constant less than one that it describes the *AC* component contribution to the dispersive region [8,9]. It is used to differentiate between dynamical charge transport mechanisms like quantum mechanical tunneling (QMT), non-overlapping small polaron tunneling (NSPT), overlapping-large polaron tunneling (OLPT), and correlated barrier hopping (CBH) [10]. However, there are severe issues concerning the validity of the UPL, as pointed out by Papathanassiou et al. [11]:

(i) It was discovered experimentally that the *n* exponent of the UPL can be greater than unity, and no physical arguments can be advanced to put a limit on its value [12–14],

(ii) the *n* exponent of the UPL is frequency dependent [5,7],

(iii) the UPL has no upper frequency limit, which is in contradiction with experimental observations ([11], [12], [13]).

Moreover, it is worth noting that both electron and ion conducting materials can display UPL behavior in their *AC* conductivity, which indicates that the charge transport properties are unrelated to the constituent units and are more likely connected to the morphology of the conducting network of these materials.

Based on physical hypothesis, an analytical model was initially developed by Papathanassiou et al. [11] and complemented by Liang et al. [18]. This model, hereafter referred to as the analytic model, allows to describe the frequency dependent conductivity of disordered materials. It is based on a spatial distribution of conduction paths along which the electric charges flow. The model qualitatively reproduces the observed frequency dependent conductivity of a wide range of polymers and composite disordered materials [15–18]. Indeed, dynamical conductivity described by power laws with exponents greater than unity is physically acceptable within this model and has been observed in some cases ([11], [12], [13]). The saturation of conductivity at high frequency is also predicted and experimentally observed [12–15]. Another feature of this analytic model is that the exponents of the power law do not accumulate to some critical value (around 0.6–0.7, as suggested by [12–15]).

Nonetheless, some of the analytic model must be discussed: (i) the distribution of path lengths is assumed to follow a log-normal function that does not depend on frequency, (ii) The conductance and capacitance associated with a conducting path are inversely proportional to the path length, (iii) only the

self-capacitance of conducting paths was considered, while charge accumulation in adjacent paths, which may also contribute to the capacitance, was ignored.

In this work, we investigate the charge transport properties of nano-composites materials consisting of metal nanoparticles embedded in a polymer matrix. Our approach is based on numerical simulations of the dynamical charge transport properties of a network made up of *N* elementary electric nano-circuits. It can be implemented in numerical solvers using the continuity of the electric current equations. The latter are discretized throughout the network, yielding *NxN* equations which can be solved according to Kirchhoff's law. This approach has been developed theoretically [19,20] and applied to MOS (Metal Oxyde Semiconductor) devices [21], magnetic sensors, quantum Hall effect-based devices [18,19] and to electric networks using commercial simulation software [24–26]. However, these models either do not take into account the actual spatial distribution of the elementary circuits (i.e., positions within the network) or are unable to describe the local properties of the charge transport in a nano-circuit.

Starting with an elementary electrical circuit describing the inter-particle charge transport properties at the nano-scale, we show that it is possible to determine the microscopic electrical resistance *R* and capacitance *C* of the entire network (Figure 1a). Because it can handle the actual spatial distribution of the nanoparticles, the numerical approach is versatile and can describe percolation and localization due to disorder effects. It also allows for the analysis and classification of conduction paths based on their length distribution and frequency dependence. It is therefore a powerful tool for testing the validity of analytical models. To the best of our knowledge, no such comparison of numerical simulations and analytical modeling has ever been performed in the context of impedance spectroscopy of composite nano-materials. Furthermore, the numerical simulations presented in this work are based on a general approach because the resistance and capacitance of an elementary circuit can be adapted to any particular system. One important motivation for this research is to determine whether it is possible to address the microscopic electrical properties of nano-particle networks investigated experimentally by impedance spectroscopy using nano-circuit building blocks.

Results and discussion:

1 – Analytical modeling:

According to the analytical model [11,15–18] the response of a disordered system to an applied *AC* field is irrelevant to its constituting elementary units and the way that they build up. They merely has to do with the morphology of the conducting network. Electric charges move in a network made up of conduction paths of varying lengths, regardless of the identity of the basic units or how they are built up. A qualitative description of a polymer network in this approach consists of a group of polymer chains of varying lengths, with conformational disorder and random orientation. Charge carriers can hop along a

chain (intra-chain transfer) and over cross-linked chain clusters (inter-chain transfer). The latter is determined, by the degree of chain coupling. As a result, charge carriers flow in a network formed by conductive paths of varying lengths, characterized by a statistical distribution determined, in part, by the material's synthesis procedure. It is worth noting that a single path does not necessarily correspond to a single chain, but can involve a cluster of coupled chains. A path can be long enough to connect the electrical contacts on the sample's opposite sides. Shorter paths are more likely to end in a dead end. The characteristic travel distance L_C of charges moving along a conductive path during half a period of the sine wave describing the *AC* electric field is defined as [18]:

Eq. 1 $$L_c(\omega) = \frac{2.v}{\omega}$$

where υ is the charge carrier velocity along the conducting path and ω is the angular frequency.

Because charges travel over distances of the order of L_C, the latter can be interpreted as a cut-off distance. Depending on the length L_k of the conducting path, two limiting cases can be distinguished:

(i) for $L_k > L_C$ (long clusters), the charges move freely along the conducting path k. Paths connecting the contact electrodes contribute to the *DC* conductance G_{DC}. Their length is equal to or larger than the inter-electrode separation. Whereas paths with dead-ends (*i.e.* non-connecting) and longer than L_C are responsible for the frequency dependent conductance $G_{AC}(\omega)$. Their length can be shorter, comparable or even larger than the inter-electrodes separation. With these assumptions, the total conductance can be written as:

Eq. 2 $$G(\omega) = G_{DC} + G_{AC}(\omega) = G_{DC} + \sum_{L_k \geq L_c(\omega)} G_k(L_k)$$

where $G_k(L_k)$ is the conductance of a path with length L_k.

(ii) for $L_k < L_C$ (short clusters), the charges cannot move freely and accumulate at the ends of the conducting path, which behaves as a capacitor and gives rise to polarization effects. The contribution of such paths, to the overall capacitance, is expressed as:

Eq. 3 $$C(\omega) = \sum_{L_k \leq L_c(\omega)} C_k(L_k)$$

Considering uncorrelated paths (*i.e.* random disorder), Papathanassiou et al. and Liang et al. [18]: assumed a continuous log-normal distribution of conduction path lengths:

Eq. 4 $$f\left(log\, \tilde{L}\right) = \frac{1}{\sqrt{2\pi}.s}.exp\left(-\frac{(log\, \tilde{L} - log\, \tilde{L}_0)^2}{2s^2}\right)$$

where $\tilde{L} = {}^{L}/_{L_{min}}$ is a normalized dimensionless path length defined as the ratio between the path length L and a minimum path length L_{min}. The latter is taken as the size of an elementary building block. $\tilde{L}_0 = {}^{L_0}/_{L_{min}}$ is the normalized mean path length, L_0 being the length of the most abundant paths. s is the dimensionless parameter defining the width of the log-normal distribution. The full width at half maximum (FWHM) of the path length distribution, having the dimension of a length, is given by:

Eq. 5 $$\Delta L = 2L_0.sinh\left(s.\sqrt{2.log2}\right)$$

As underlined above, an important assumption of the analytical model is that the conductance and capacitance associated to a given conducting path are inversely proportional to its length ($G_k \propto L_k^{-1}$ and $C_k \propto L_k^{-1}$). Within this assumption, Eq. 2- Eq. 4 lead to (see SI):

Eq. 6 $$G(\omega) = G_{DC} + G_0.\int_{log(\tilde{L}_{c(\omega)})}^{log(\tilde{L}_{max})} \frac{1}{\sqrt{2\pi}.s}.exp\left(-\frac{(y-log\,\tilde{L}_0)^2}{2s^2}\right).dy$$

Eq. 7 $$C(\omega) = C_0.\int_{0}^{log(\tilde{L}_{c(\omega)})} \frac{1}{\sqrt{2\pi}.s}.exp\left(-\frac{(y-log\,\tilde{L}_0)^2}{2s^2}\right).dy$$

where $G_0 = N.S.\sigma$ and $C_0 = N.S.\varepsilon$ are respectively the overall conductance and capacitance of the *N* paths forming the conducting network; σ and ε are respectively the conductivity and permittivity of a conducting cluster and *S* is the network cross section. The bounds of the integrals (Eq. 6 and Eq. 7) are defined by the normalized critical length $\tilde{L}_{c(\omega)} = {L_c(\omega)}/{L_{min}}$ and the normalized maximum length $\tilde{L}_{max} = {L_{max}}/{L_{min}}$; $L_{max}$is set to several inter-electrode distances to ensure full convergence of the integral (Eq. 6).

The results of the numerical simulations of the charge transport properties of a network formed by interconnected building blocks of elementary electrical circuits will be compared to the conductance and capacitance deduced from the analytical model presented above.

2 – Numerical simulations:

The approach developed in this work is based on numerical simulations of the dynamical charge transport properties of a network composed of elementary electric nano-circuits (Figure 1).

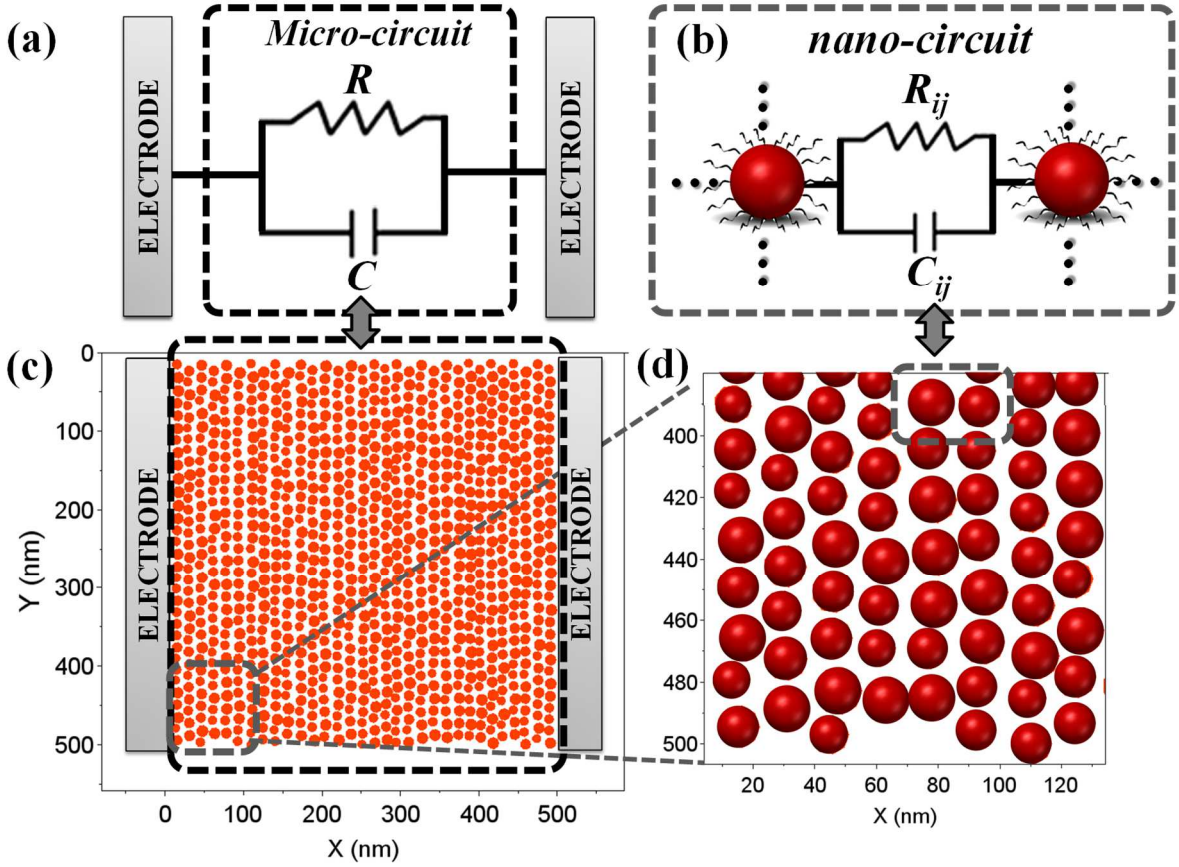

Figure 1: (a) microscopic resistance R and capacitance C of the microscopic circuit (c,d) resulting from the charge transport over the whole network formed by inter-connexion of elementary nano-circuits (b). The latter are formed by inter-particle resistance R_{ij} and capacitance C_{ij}. The size of the simulated network is 500 nm x 500 nm containing around 1024 nanoparticles; 15% size and position fluctuations are included to account for structural disorder.

Each circuit is a *(i,j)* pair of first neighbor nanoparticles characterized by an inter-particle resistance R_{ij} and capacitance C_{ij} (Figure 1b). The latter depend on the characteristics of the nanoparticle network (size, shape, separation and spatial distribution), on the surrounding medium (dielectric properties) as well as on temperature and eventually on an applied external stress.

Calculations were performed for a system which has been investigated experimentally in previous works [27]. It consists in a single layer of spherical gold NPs (14 nm average size) arranged in a regular hexagonal lattice. The separation between neighboring NPs is set to the length (1.2 nm) of the stabilizing C_{12} molecules [27]. The simulated network is composed approximately of 1024 NPs (Figure 1c); a number large enough to generate thousands of conducting paths and at the same time keep within tractable computation time. Moreover, a size distribution linewidth of 15% of the average NP size and positions (with respect to positions of NPs in the regular array) was introduced in the network (Figure 1c) to mimic the lattice disorder effects [28].

It is worth to mention that the results of the numerical simulations presented in this work are quite general and do not depend critically on the characteristics of the elementary building blocks forming the network.

Each *(i,j)* pair of nanoparticles located at positions (r_i, r_j) of the 2D network gives rise to a parallel equivalent electrical nano-circuit (Figure 1b) with admittance matrix element:

Eq. 8 $$\chi_{ij} = 1/R_{ij} + jC_{ij}\omega$$

where R_{ij} and C_{ij} are the inter-particle resistance and capacitance, respectively.

In our case, assuming that charge transport occurs through quantum tunnelling between first neighbour nanoparticles, the resistance R_{ij} is given by [28–30]:

Eq. 9 $$R_{ij} = k_R . e^{\xi(V_{ij},T)}$$

where k_R is the inter-particle resistance at the touching limit, *i.e.* for vanishing inter-particle gap distance l_{ij} ; ξ accounts for the electron tunnelling effect [28–30]:

Eq. 10 $$\xi = \beta l_{ij} - ln\left(g(E_c, T, V_{ij})\right) \text{ with } g(E_c, T, V_{ij}) = \frac{1}{eV_{ij}}\left(-\frac{E_C - eV_{ij}}{1-e^{(E_C - eV_{ij})/k_B T}} + \frac{E_C + eV_{ij}}{1-e^{(E_C + eV_{ij})/k_B T}}\right)$$

As detailed in references [29,31], ξ depends on the tunnelling decay constant β (around 3 nm^{-1} for the considered system [29,32]), and on the number of tunnelling states $g(E_c, T, V_{ij})$ which is determined by the Coulomb charging energy E_C, *c.a.* 20 meV [28,29]), the temperature T and the voltage V_{ij} between first neighbour nanoparticles.

The inter-particle capacitance C_{ij} is given by [31,33]:

Eq. 11 $$C_{ij} = \pi\varepsilon d . ln(1 + d/l_{ij})$$

Where d is the nanoparticle diameter, ε is the permittivity of the surrounding medium (*i.e.* of the ligand molecules in our case).

The complex admittance matrix [Y] is constructed assuming that all first neighbour nanoparticles are located within a ring centered on the considered nanoparticle. The current flowing throughout the NP network is computed by solving numerically the matrix equation [34]:

Eq. 12 $$[\boldsymbol{V}] = [\boldsymbol{Y}]^{-1}[\boldsymbol{I}]$$

where *[V]* and *[I]* are, respectively, the voltage and the injected current vectors, and *[Y]* is the complex admittance matrix of which non-diagonal and diagonal terms are, respectively, $Y_{ij} = -\chi_{ij}$ for $i \neq j$, and $Y_{ii} = \sum_j \chi_{ij}$; the latter being the total admittance connected to node *i* [35].

The overall microscopic admittance of the network formed by the interconnected nano-circuits is $Y_0 = V_0/I_0$ where $V_0(\omega)$ is the voltage vector at the collecting electrode and $I_0(\omega)$ is the injected current at the injection electrode. Finally, the conductance *G* and susceptance *S* of the network are obtained as $G(\omega) = Re(Y(\omega))$, and $S(\omega) = Im(Y(\omega))$, *respectively.* It is worth to mention that the numerical model is able to handle disorder (point defects and dislocations in the NPs network) as well as strain effects (due to an

applied external stress) on the charge transport properties of the NPs assembly.

4 – Comparison between analytical model and numerical simulations:

The *AC* conductance $G_{AC}(\omega) = G(\omega)-G_{DC}$ and capacitance $C(\omega) = S(\omega)/\omega$ were normalized to their respective maximum values to allow for a direct comparison of the charge transport properties calculated using the analytical model and the numerical simulations (Figure 2). In this way, changes in the electrical response due to system size (number of interconnected nanoparticles, length of electrodes, distance between electrodes) are eliminated. Furthermore, the normalized conductance and capacitance shown in Figure 2 are plotted as a function of the logarithm of the normalized angular frequency ω/ω_0, where ω_0 is the frequency at half maximum of the conductance, and is determined only by L_0 and $L_c(\omega)$ in the analytical model (Eq. 1) and by the electrical characteristics of each nano-circuit in the numerical simulations (Eq. 9 and Eq. 11). This normalization procedure preserves the general nature of both the analytical modeling and the numerical simulations, allowing them to be applied to a variety of disordered nano-structured materials. It also restricts the adjustable parameters of the analytic model to the width (*i.e.* parameter *s*) of the log-normal distribution of path lengths which defines the frequency-dependent line-shape of the normalized conductance and capacitance.

Figure 2 shows that the analytical model and the numerical simulations both account for the frequency dependence of the *AC* conductance and capacitance with the three previously mentioned distinct regions: nearly constant low-frequency *DC* regime, strong frequency variation around ω_0 and saturation at high frequency, resulting in an *AC* plateau in the conductance and vanishing capacitance. As shown in Figure 2, there is a good agreement between the numerically simulated conductance and capacitance and the ones calculated using the analytical model (Eq. 6 and Eq. 7) for $s \approx 1$ which corresponds to the width of the log-normal distribution of conducting path lengths in the numerically investigated nano-particle network, as described by the analytical model.

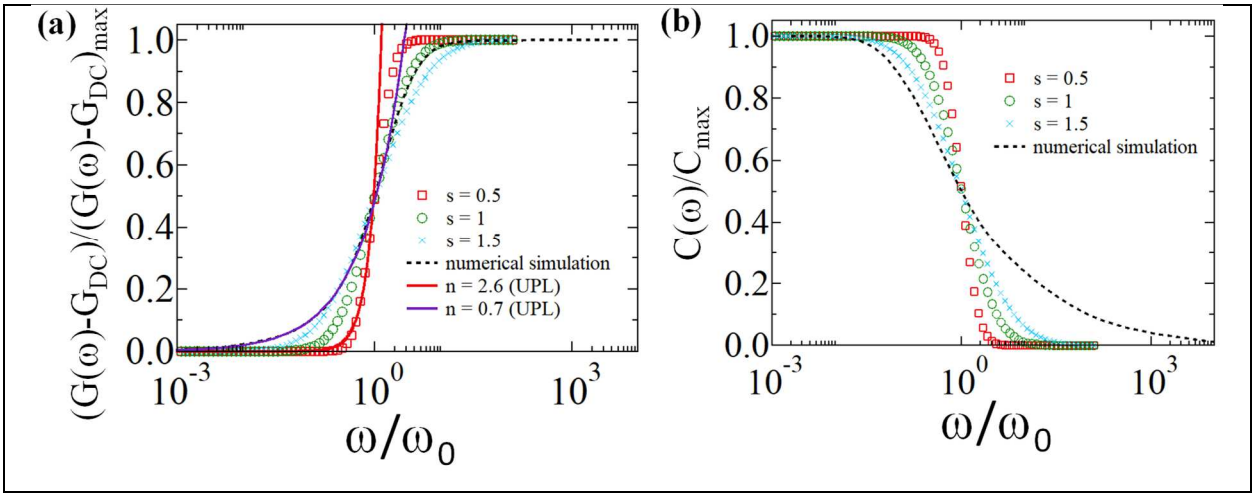

Figure 2: Comparison between (a) the normalized AC conductance $(G(\omega)-G_{DC})/(G-G_{DC})_{max}$ and (b) capacitance $C(\omega)/C_{max}$ calculated using the numerical simulations (dotted black line) and the analytical

model with a broadening parameter of the log-normal distribution s = 1.5 (crosses), 1 (circles) and 0.5 (squares). The UPL fitted to the analytical model with parameter s = 0.5 and to the numerical simulations of the conductance are shown in solid lines. The corresponding fractional exponents c.a. n = 2.6 and 0.7, respectively.

However, there are some inconsistencies between the numerically simulated and the analytically computed conductance and capacitance line-shapes (Figure 2). In particular, the analytic model, overestimates the high frequency capacitance because it ignores the capacitance formed by adjacent paths, whereas numerical simulations account for both the self-capacitance of a given path and the geometric capacitance formed by its first neighbor paths via the inter-particle capacitance term (Eq. 11), as will be discussed in more detail below. Furthermore, as it will be shown, the width of the log-normal distribution (parameter *s* in Eq. 4) is substantially frequency dependent, which is not taken into account in the analytical model and may influence the frequency dependent conductance and capacitance line shapes.

Furthermore, Nyquist plots are commonly used in impedance spectroscopy experiments as they allow for determining the equivalent electric circuit of a conducting system. Figure 3 shows Nyquist plots based on the frequency dependent conductance and capacitance calculated using the analytic model (Eq. 6 and Eq. 7) and on the numerical simulations (Eq. 12). The real $Z'(\omega) = {}^{1}/_{G(\omega)}$ and imaginary $\mathrm{Z''}(\omega) = {}^{1}/_{\omega \mathrm{C}(\omega)}$ parts of the impedance were normalized to their maximum values to allow for a direct comparison between the analytical model and the numerical simulations. In this way, the normalized impedance is determined solely by the nature of the electrically equivalent circuit and not by the parameters of the log-normal distribution of path lengths (Eq. 4) or by the nano-circuit resistance and capacitance (Eq. 8).

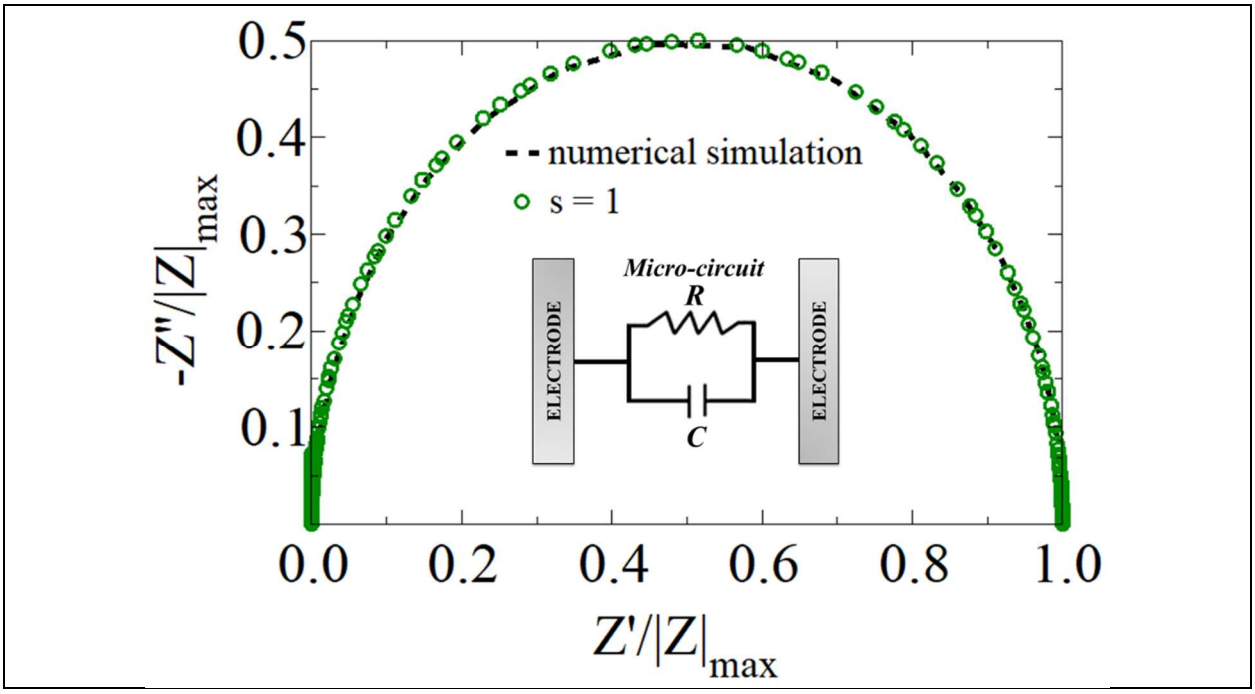

Figure 3 : Comparison between normalized Nyquist impedance plots (i.e. $Z'/|Z|_{max}$ versus $-Z''/|Z|_{max}$) calculated (a) using the analytical model based on a log-normal distribution of conducting path lengths with s = 1 (black dots) and (b) using the numerical simulations of the interconnected nano-circuit network shown in Figure 1.

The analytic model and the numerical simulations both produce Nyquist plots with a semicircle shape which is characteristic of an equivalent circuit composed of frequency-independent parallel resistance *R* and capacitance *C*. The *R* and *C* parameters are the low frequency resistance and capacitance, respectively $R = {}^{1}/_{G_{DC}}$ and $C = C_{max}$. The resonance frequency of the parallel circuit is $\omega_0 = {}^{1}/_{RC}$. These findings are consistent with experimental impedance spectroscopy data from a variety of nano-composite materials, including self-organized metal nanoparticle assemblies [33], polymers (PBLG)/metal (Pt) nano-composites [36], and granular phase change materials [37]. At low frequencies $\omega \ll \omega_0$ the susceptance is very small compared to the conductance ($\omega C << R^{-1}$) and the capacitors can be regarded as open circuits; the electrical system is thus dominated by the equivalent resistance *R* of the elementary resistances along the different percolation paths across the network (Figure 2). At intermediate frequencies $\omega \approx \omega_0$, conductance and susceptance are comparable ($\omega C \sim R^{-1}$). The conductance increases with increasing frequency in this frequency range, which can be described by a UPL, and has been suggested to be linked to the capacitive components of the network [9,24]. At high frequencies $\omega \gg \omega_0$, the susceptance far outweighs the conductance ($\omega C >> R^{-1}$) and the capacitors act as short circuits between conducting paths, increasing the overall conductance. It is worth noting that our simulations show non-divergent conductance at high frequencies because the proportion of capacitors (37%) in our network is significantly less than the mathematically required 50% for percolation in a two-dimensional (2D) network [38,39]. As a result, the conductance of conducting paths is constrained by the presence of resistors, which determine

the network's overall conductance. Moreover, the numerical simulations show that the frequency dependence of the conductance and capacitance is universal, as indicated by Bouamrane and Almond [5,20,21] who showed that the UPL is an « emergent property », *i.e.* a well-defined characteristic of the electrical response that appears to be independent of the arrangement of the resistors and capacitors within the network. However, the exponent of the UPL depends on the width of the distribution of the conducting paths (Figure 2) and can thus take values greater than 1, as demonstrated experimentally [8–11] and analytically [7,14]. Fitting the UPL to our numerically simulated conductance (Figure 2) yields a fractional exponent *c.a.* 0.7 for the network with 15% nanoparticle size and position dispersion whereas fitting the UPL to the analytic model leads to a fractional exponent increasing from n = 0.65 to 2.6 for log-normal width parameter decreasing from s = 1.5 to 0.5 (Figure 2).

Both the analytic model and the numerical simulations are thus capable of capturing the essential physics of the charge transport properties of complex nano-composite materials in terms of conducting paths (analytic model) or elementary nano-circuits (numerical simulations). However, numerical simulations have a superior capability of reconstructing conduction paths and can thus address the distribution of path lengths. Indeed, one important assumption of the analytic model is that the lengths of the conducting paths follow a log-normal distribution. In the following sections, we will focus on this point and show that the distribution of path lengths is frequency dependent and can deviate significantly from a log-normal distribution.

The length of a conducting path and its electric characteristics are extracted from the numerical simulations as follows: the spatial distribution of the nano-junctions formed by each pair of first neighbor nanoparticles is obtained from the location of the nanoparticles within the network. Then, only the paths connecting the injection and the collection electrodes are selected. These percolation paths are directly involved in the measured conductivity; non-connecting paths (*i.e.* with dead ends) are present and may influence the charge transport and its frequency dependence, but only indirectly. Finally, the length L_k of each individual k-path is calculated and its impedance $1/G_k$ is calculated as the sum of the local impedances of the nano-junctions forming the conduction the path. The so-obtained path lengths and conductances can be then represented as histograms. Figure 4 shows the path length histograms calculated at low (Figure 4a) and high (Figure 4b) frequencies.

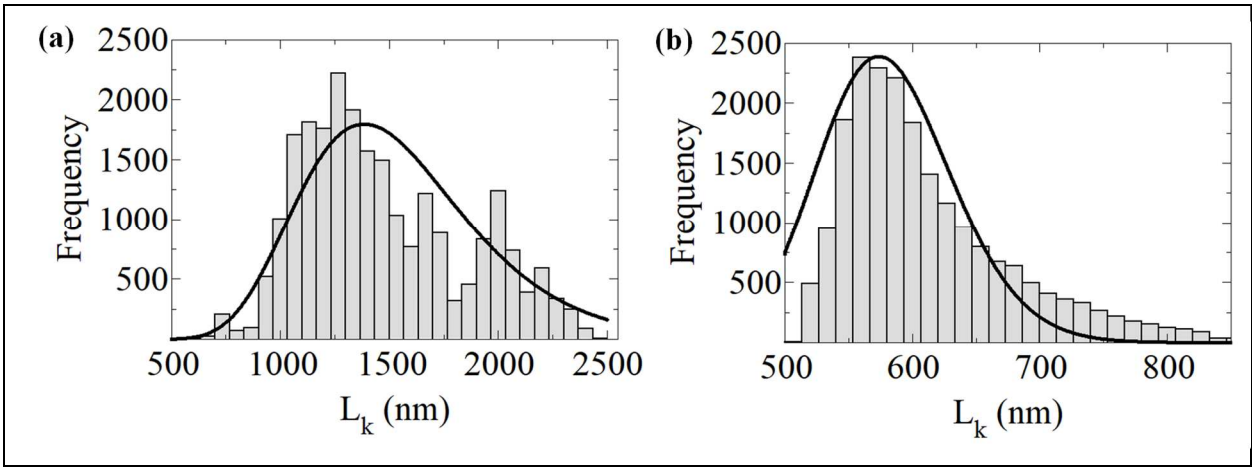

Figure 4 : Histograms of conduction path lengths extracted from the numerical simulations of a hexagonal lattice network (500 nm x 500 nm) formed by gold nanoparticles including 15% size fluctuations. The simulations were performed at (a) low ($\omega/\omega_0 = 10^{-3}$) and (b) high frequency ($\omega/\omega_0 = 10^{4}$). Continuous line curves are fits of path length log-normal distribution functions (Eq. 4) to the path length histograms using parameters (L_0=1400 nm, ΔL~ 900 nm) corresponding to s~0.3 in (a) and (L_0=600 nm, ΔL~ 175 nm) corresponding to s~0.12 in (b).

The dependence of the path length histograms on frequency originates from the capacitance of the nano-circuits (Eq. 8). The capacitive contribution to the conductance has a logarithmic variation with inter-particle distance (Eq. 11) whereas the resistance contribution decreases exponentially with increasing gap between the nanoparticles (Eq. 9). Since the capacitive contribution dominates at high frequency $\omega/\omega_0 = 10^4$, this leads to longer paths compared to the low-frequency case $\omega/\omega_0 = 10^{-3}$ where the resistance favours the shorter paths. At high frequency (Figure 4b), the path length histogram follows rather well a log-normal distribution function with parameters L_0 = 600 nm and ΔL ~ 175 nm (corresponding to s ~ 0.12 in Eq. 5). At low frequency (Figure 4a), the path length histogram is shifted upward to larger path lengths and spreads over a broader range. The low frequency histogram is not well described by a log-normal distribution because of the strong fluctuations of the nano-circuit resistance with inter-particle distance (Eq. 9).

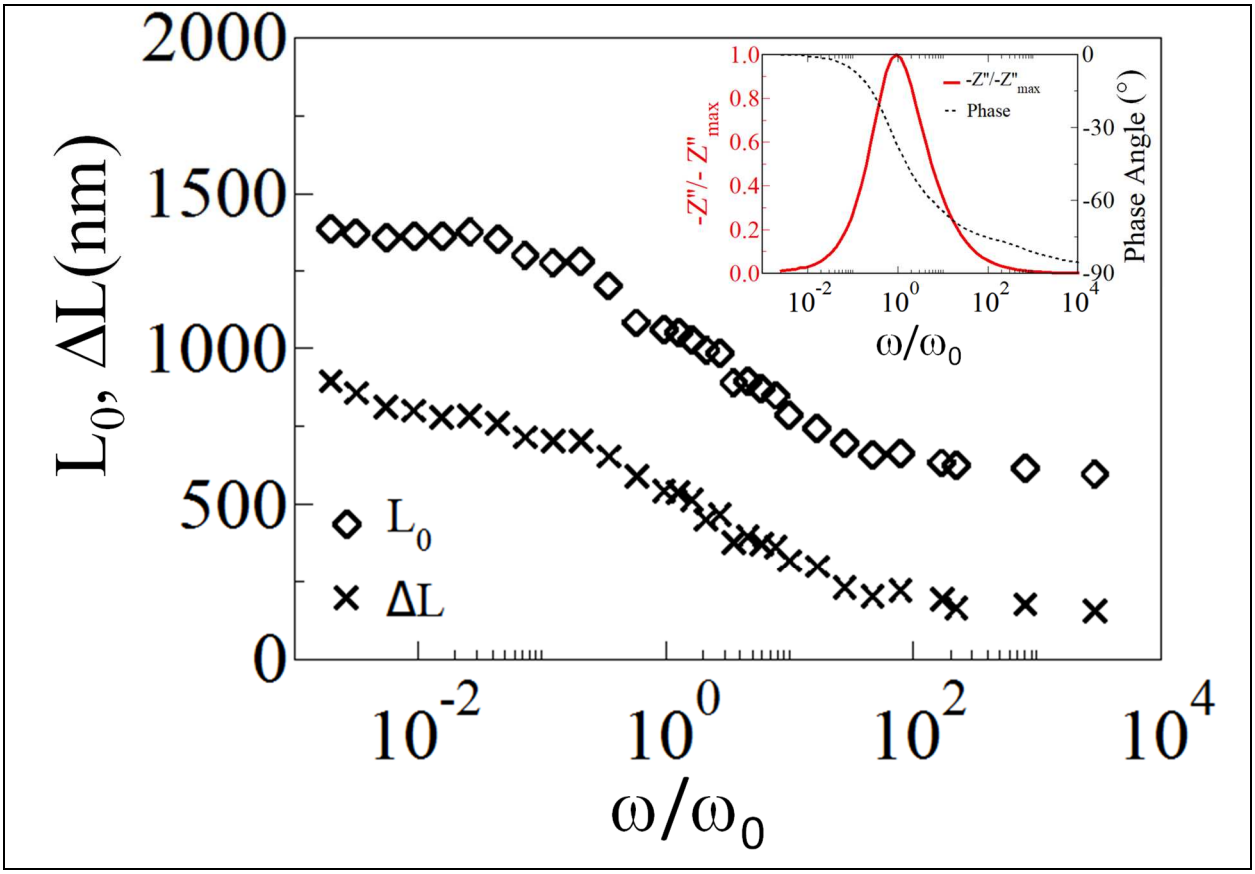

Figure 5 : (a) Frequency dependence of the length L_0 and FWHM ΔL of the log-normal distribution fitted to the path length histograms extracted from the numerical simulations of the investigated network. The frequency is in log scale. (insert) resonance curve of the normalized imaginary part of the impedance obtained using the numerical simulations. The resonance frequency is $f_0 = 10^4$ Hz for the investigated network.

Figure 5 displays the frequency dependence of parameters L_0 and ΔL of the log-normal distribution fitted to the path length histograms. As already noticed in Figure 4, L_0 and ΔL clearly decrease with increasing frequency. This finding indicates that the length distribution of the conducting paths is in fact frequency dependent which was not considered in the analytic model. Moreover, the frequency variation of L_0 does not follow the $1/\omega$ dependence (Eq. 1) assumed in the analytic model. L_0 and ΔL rather follow an S-shaped frequency dependence (Figure 5) with a clear change of the electric characteristics from resistive (at low-frequency) to capacitive (at high frequency) behavior around the resonance frequency $f_0 = {}^1/_{2\pi RC}$ of the microscopic electric circuit formed by the inter-connected nano-circuits. In the investigated network, $f_0 = 10^4$ Hz which corresponds to the maximum of $-Z''(\omega)$ and a 45° phase shift between the resistive and capacitive components of the equivalent parallel circuit as shown in the inset of Figure 5.

The frequency dependence of L_0 and ΔL is partly responsible for the difference between the frequency dependent conductance and capacitance calculated using the analytic model and the numerical simulations shown in Figure 2. Indeed, the broadening parameters s of the log-normal distribution fitted

to the path length histograms (Figure 4) are lower than those (s~1) deduced from the analysis of the frequency dependent conductance and capacitance (Figure 2). This is due to *(i)* the fact that the frequency dependence of the log-normal distribution is not considered in the analytical model (Eq. 4), *(ii)* the deviation of L_0 from the $1/\omega$ dependence (Eq. 1), and *(iii)* the dependence of the conductance of an individual path on its length (used in Eq. 6 and Eq. 7).

Indeed, one important assumption of the analytical model is that the conductance and capacitance of a particular path are inversely proportional to its length (implicit in Eq. 6and Eq. 7). To test the validity of this assumption we have extracted, from the numerical simulations, the dependence of the conductance and capacitance on path length. This is performed as follows: once Eq. 12 is solved numerically, a particular length, in the frequency-dependent path length histogram (Figure 4), is selected. Several different conducting paths with this same length occur in the network. The impedance of each path is calculated as the sum of the impedances of the nano-circuits formed by first neighbour nanoparticles along the path. Hence, in the numerical simulations, several mesoscopic conductance and capacitance values are associated to a path length. Figure 6 depicts the change in conductance and capacitance as a function of path length derived from the numerical simulations performed at the microscopic circuit's resonance frequency f_0.

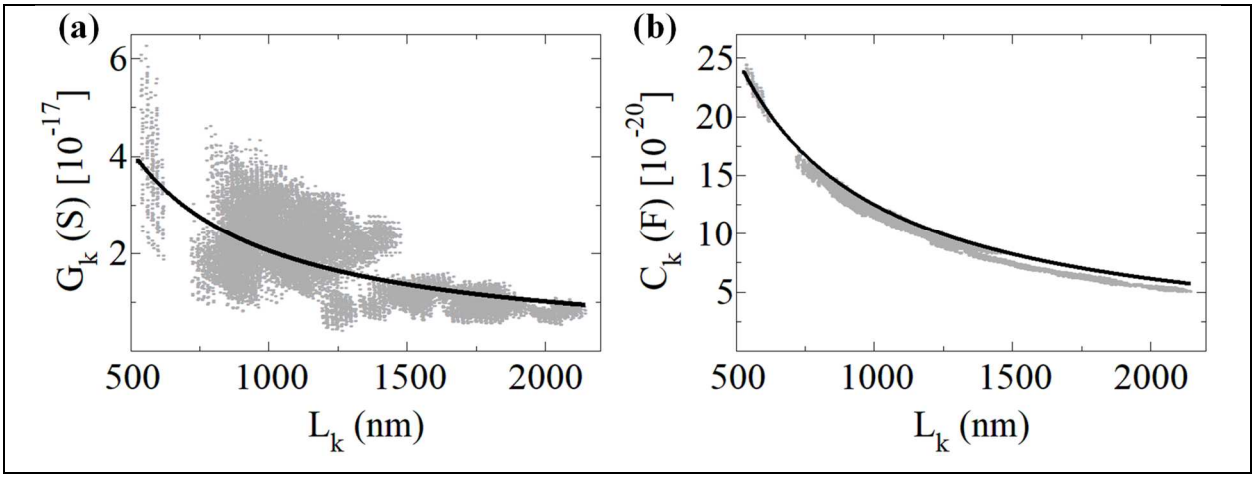

Figure 6 : (a) Conductance and (b) capacitance as a function of path length for the nano-circuit network with 15% nanoparticle size and position dispersion (dots) and for the perfectly ordered network (full line) at the resonance frequency $f_0 = 10^4$ Hz.

Because of the strong (exponential) dependence of the nanoscopic tunnelling resistance on the inter-particle distance (Eq. 9), the values of the conductance associated to a given path length are scattered over a wide range (Figure 6). In contrast, the values of the capacitance exhibit less scattering because of the weaker (logarithmic) dependence of the nanoscopic capacitance on interparticle distance (Eq.11). The conductance and capacitance do decrease with increasing path length (Figure 6). In fact, we have discovered that their dependency on path length and frequency are highly influenced by the degree of disorder. As a matter of fact, we found that the mesoscopic conductance and capacitance decrease as

the inverse path length, as assumed in the analytical model (Eq. 6 and 7), only in the case of a perfectly ordered nanoparticle network (full lines in Figure 6).

The existence of conducting paths and their properties are assumed in the analytic model. In the numerical simulations, the conducting paths emerge as a result of the solutions of Eq. 12. They can be viewed, compared, and classified which allows for a better understanding of the charge transport properties. Figure 7 displays conduction paths chosen from the path length histogram generated at the network's resonance frequency $f_0 = 10^4$ Hz.

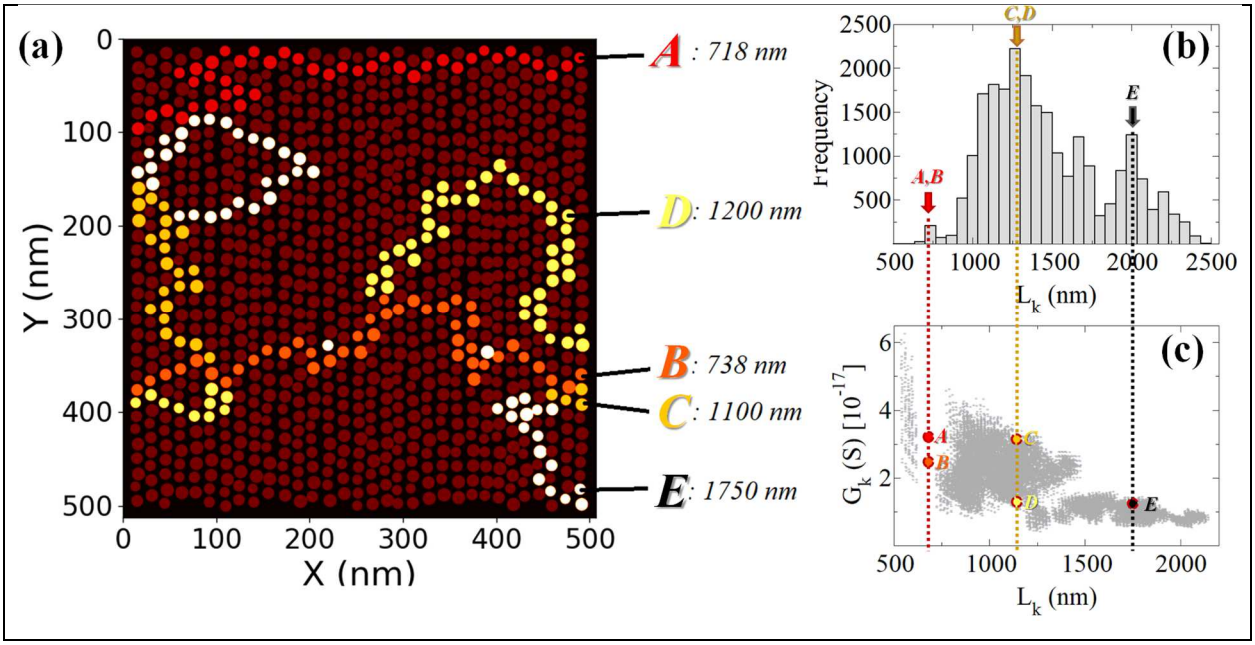

Figure 7 : (a) Spatial distribution of five paths selected in the path histogram (b) calculated at the resonance frequency $f_0 = 10^4$ Hz: A = (G_A=3.19x10^{-17} S, L_A=718 nm), B = (G_B=2.56x10^{-17} S, L_B=738 nm), C = (G_C=3.12x10^{-17} S, L_C=1100 nm), D = (G_D=1.3x10^{-17} S, L_D=1200 nm) and E = (G_E=1.26x10^{-17} S, L_E=1750 nm) (c) path conductance as a function of path length extracted from the numerical simulations.

We would like to emphasize that all of the conducting paths in the numerical simulations are connecting paths (Figure 7). They start at the injection electrode and terminate at the collection electrode. So, the minimum path length is equal to the inter-electrode distance (500 nm in our case). Conduction paths A and B in Figure 7 correspond to short connections between the electrodes; their lengths (718 and 738 nm, respectively) are comparable to the inter-electrode distance (500 nm). The path labelled E in Figure 7 contains a greater number of nanoparticles; its length (1750 nm) is nearly three times larger than the inter-electrode distance. The paths labelled C and D in Figure 7 are representative of the most common paths. Their length is nearly twice as long as the distance between the electrodes. Paths of varying lengths may share common segments: for example, paths (D, B) and (C, B, E). Paths A and E interact with one another. They do not share common segments, but three of their nanoparticles are first neighbours (around *x*=100 nm, *y*=100 nm coordinates) which affects the impedance of both paths. Such interaction is responsible for inter-path conductance and capacitance (as suggested in the discussion of Figure 2). Paths of the same length can have vastly different conductances, as shown in Figure 6. For

example, paths C and D (Figure 7) have very similar lengths but very different conductances. Path C has nearly three times the conductance of path D. Finally, the conducting paths are frequency dependent. The low frequency conducting paths displayed in Figure ESI 1 are longer than the high frequency ones in agreement with the path length histograms of Figure 4.

CONCLUSION

In conclusion, we compared analytic models and numerical simulations of the charge transport properties in networks of self-organized metal nanoparticles. The electric properties were implemented in the numerical simulations at the nanoscale by accounting for tunneling resistance and mutual capacitance, formed by neighboring nano-particles. These nano-circuits serve as the fundamental building blocks of the network micro-circuit. We found a general agreement between the electric properties of the nano-particle network predicted by the numerical simulations and the analytic model. The agreement with the UPL is limited to the low-frequency range as the UPL is unable to account for the high frequency saturation of the conductance.

The analytic models are based on assumptions about the electric properties of conducting paths and their statistical distribution. The conducting paths, on the other hand, can be extracted and investigated in numerical simulations at both the individual (path associated impedance) and global levels (path length histograms), allowing the assumptions of the analytic models to be addressed. In particular we found that *(i)* The path length histograms are frequency dependent and they more or less follow the log-normal distribution of the analytic model only at high frequencies where the capacitive response of the conducting paths dominates. *(ii)* The conductance and capacitance of a conducting path are inversely proportional to its length only for a perfectly ordered nano-particle network, as assumed in the analytic model. Fluctuations in nanoparticle size and position result in scattered conductance values for a given path length. Conducting paths of the same length can have vastly different electric properties which was not considered in the analytic model. *(iii)* All of the investigated paths in the numerical simulations are connecting paths, *i.e.* percolating paths with lengths greater than the inter-electrode separation. To introduce charge accumulation and capacitive effects, non-connecting paths do not need to be invoked as in the analytic model [7,14]. Nevertheless, they could be present in the numerical simulations and may influence the conductance and susceptance of a conducting path.

Once the local electric properties (resistance and capacitance) of a composite material are known, the approach developed in this work can be applied to predict its macroscopic electric properties (frequency dependent conductance and susceptance). The spatial arrangement and relative positions of the inter-particles within the network directly determine the local resistance and capacitance, which is an important feature of the numerical simulations presented in this work. As a result, both disorder and strain effects imposed on the network can be accounted for. Furthermore, using the numerical tool

developed in this work, photo-induced charge generation within the nanoparticles and the surrounding medium can be addressed by supplementing the local electric resistance and capacitance with appropriate electric model components describing the light-matter interaction.

SUPPLEMENTARY MATERIAL:

Mathematical details of the analytical model and figures showing low and high frequency conduction paths.

ACKNOWLEDGMENTS :

The authors would like to express their gratitude to B. Viallet for initiating the Scilab numerical simulator on a nanoparticle network. Financial support from Agence Nationale de la Recherche (NAMAS through the EUR grant NanoX no. ANR-17-EURE-0009 in the framework of the Programme des Investissements d'Avenir.

DATA AVAILABILITY:

Data available on request from the authors

REFERENCES

[1] J. S. Steckel, P. Snee, S. Coe-Sullivan, J. P. Zimmer, J. E. Halpert, P. Anikeeva, L.-A. Kim, V. Bulovic, and M. G. Bawendi, *Color-Saturated Green-Emitting QD-LEDs*, Angew. Chem. Int. Ed. **45**, 5796 (2006).

[2] J. E. Millstone, S. J. Hurst, G. S. Métraux, J. I. Cutler, and C. A. Mirkin, *Colloidal Gold and Silver Triangular Nanoprisms.*, Small Weinh. Bergstr. Ger. **5**, 646 (2009).

[3] M. V. Jarosz, V. J. Porter, B. R. Fisher, M. A. Kastner, and M. G. Bawendi, *Photoconductivity Studies of Treated CdSe Quantum Dot Films Exhibiting Increased Exciton Ionization Efficiency*, Phys Rev B **70**, 195327 (2004).

[4] H. Nakanishi, K. J. Bishop, B. Kowalczyk, A. Nitzan, E. A. Weiss, K. V. Tretiakov, M. M. Apodaca, R. Klajn, J. F. Stoddart, and B. A. Grzybowski, *Photoconductance and Inverse Photoconductance in Films of Functionalized Metal Nanoparticles*, Nature **460**, 371 (2009).

[5] A. G. Hunt, *Ac Hopping Conduction: Perspective from Percolation Theory*, Philos. Mag. B **81**, 875 (2001).

[6] S. Capaccioli, M. Lucchesi, P. A. Rolla, and G. Ruggeri, *Dielectric Response Analysis of a Conducting Polymer Dominated by the Hopping Charge Transport*, J. Phys. Condens. Matter **10**, 5595 (1998).

[7] J. C. Dyre and T. B. Schrøder, *Universality of Ac Conduction in Disordered Solids*, Rev Mod Phys **72**, 873 (2000).

[8] A. K. Jonscher, *A New Understanding of the Dielectric Relaxation of Solids*, J. Mater. Sci. **16**, 2037 (1981).

[9] A. K. Jonscher, *The 'Universal' Dielectric Response*, Nature **267**, 673 (1977).

[10] F. Yakuphanoglu, I. S. Yahia, B. F. Senkal, G. B. Sakr, and W. A. Farooq, *Impedance Spectroscopy Properties of Polypyrrole Doped with Boric Acid*, Synth. Met. **161**, 817 (2011).

[11] A. N. Papathanassiou, I. Sakellis, and J. Grammatikakis, *Universal Frequency-Dependent Ac Conductivity of Conducting Polymer Networks*, Appl. Phys. Lett. **91**, 122911 (2007).

[12] C. Cramer, S. Brunklaus, E. Ratai, and Y. Gao, *New Mixed Alkali Effect in the Ac Conductivity of Ion-Conducting Glasses*, Phys Rev Lett **91**, 266601 (2003).

[13] B. Louati, M. Gargouri, K. Guidara, and T. Mhiri, *AC Electrical Properties of the Mixed Crystal (NH4)3H(SO4)1.42(SeO4)0.58*, J. Phys. Chem. Solids **66**, 762 (2005).

[14] R. H. Chen, R. Y. Chang, and S. C. Shern, *Dielectric and AC Ionic Conductivity Investigations in K3H(SeO4)2 Single Crystal*, J. Phys. Chem. Solids **63**, 2069 (2002).

[15] A. N. Papathanassiou, *Novel Feature of the Universal Power Law Dispersion of the Ac Conductivity in Disordered Matter*, J. Non-Cryst. Solids **352**, 5444 (2006).

[16] A. N. Papathanassiou, J. Grammatikakis, I. Sakellis, S. Sakkopoulos, E. Vitoratos, and E. Dalas, *Low Frequency Dielectric Relaxation Phenomena in Conducting Polypyrrole and Conducting Polypyrrole-Zeolite Composites*, J. Appl. Phys. **96**, 3883 (2004).

[17] A. N. Papathanassiou, J. Grammatikakis, I. Sakellis, S. Sakkopoulos, E. Vitoratos, and E. Dalas, *Hopping Charge Transport Mechanisms in Conducting Polypyrrole: Studying the Thermal Degradation of the Dielectric Relaxation*, Appl. Phys. Lett. **87**, 154107 (2005).
[18] C. Liang, J. Gest, G. Leroy, and J.-C. Carru, *Dielectric and Conductivity Properties of Composite Polyaniline/Polyurethane Network*, J. Appl. Phys. **114**, 124106 (2013).
[19] C. Grimaldi, P. Ryser, and S. Strässler, *Anisotropic Random Resistor Networks: A Model for Piezoresistive Response of Thick-Film Resistors*, J. Appl. Phys. **92**, 1981 (2002).
[20] R. Kawakami Harrop Galvao, K. H. Kienitz, S. Hadjiloucas, G. C. Walker, J. W. Bowen, S. Figueredo Carreiro Soares, and M. C. Ugulino Araujo, *Multivariate Analysis of the Dielectric Response of Materials Modeled Using Networks of Resistors and Capacitors*, IEEE Trans. Dielectr. Electr. Insul. **20**, 995 (2013).
[21] E. Arnold, *Computer Simulation of Conductivity and Hall Effect in Inhomogeneous Inversion Layers*, in Surface Sci., Vol. 113 (1982), pp. 239–243.
[22] R. S. Popović, *Numerical Analysis of MOS Magnetic Field Sensors*, Solid-State Electron. **28**, 711 (1985).
[23] M. Ortolano and L. Callegaro, *Circuit Models and SPICE Macro-Models for Quantum Hall Effect Devices*, Meas Sci Technol 13 (2015).
[24] D. P. Almond, C. J. Budd, M. A. Freitag, G. W. Hunt, N. J. McCullen, and N. D. Smith, *The Origin of Power-Law Emergent Scaling in Large Binary Networks*, Phys. Stat. Mech. Its Appl. **392**, 1004 (2013).
[25] R. Bouamrane and D. P. Almond, *The Emergent Scaling Phenomenon and the Dielectric Properties of Random Resistor–Capacitor Networks*, J. Phys. Condens. Matter **15**, 4089 (2003).
[26] R. K. H. Galvao, S. Hadjiloucas, K. H. Kienitz, H. M. Paiva, and R. J. M. Afonso, *Fractional Order Modeling of Large Three-Dimensional RC Networks*, IEEE Trans. Circuits Syst. Regul. Pap. **60**, 624 (2013).
[27] H. Nesser, J. Grisolia, A. Mlayah, T. Alnasser, D. Lagarde, B. Viallet, and L. Ressier, *Plasmonic Photocapacitance of Self-Assembled Gold Colloidal Nanoparticle Monolayers*, Mater. Today Nano **4**, 38 (2018).
[28] H. Moreira, J. Grisolia, N. M. Sangeetha, N. Decorde, C. Farcau, B. Viallet, K. Chen, G. Viau, and L. Ressier, *Electron Transport in Gold Colloidal Nanoparticle-Based Strain Gauges.*, Nanotechnology **24**, 095701 (2013).
[29] J. Grisolia, N. Decorde, M. Gauvin, N. M. Sangeetha, B. Viallet, and L. Ressier, *Electron Transport within Transparent Assemblies of Tin-Doped Indium Oxide Colloidal Nanocrystals*, Nanotechnology **26**, 335702 (2015).
[30] M. M. A. Yajadda, K.-H. Müller, and K. Ostrikov, *Effect of Coulomb Blockade, Gold Resistance, and Thermal Expansion on the Electrical Resistance of Ultrathin Gold Films*, Phys Rev B **84**, 235431 (2011).
[31] A. J. Quinn, P. Beecher, D. Iacopino, L. Floyd, G. De Marzi, E. V. Shevchenko, H. Weller, and G. Redmond, *Manipulating the Charging Energy of Nanocrystal Arrays.*, Small Weinh. Bergstr. Ger. **1**, 613 (2005).
[32] N. Decorde, N. M. Sangeetha, B. Viallet, G. Viau, J. Grisolia, A. Coati, A. Vlad, Y. Garreau, and L. Ressier, *Small Angle X-Ray Scattering Coupled with in Situ Electromechanical Probing of Nanoparticle-Based Resistive Strain Gauges*, Nanoscale **6**, 15107 (2014).
[33] H. Nesser, J. Grisolia, T. Alnasser, B. Viallet, and L. Ressier, *Towards Wireless Highly Sensitive Capacitive Strain Sensors Based on Gold Colloidal Nanoparticles*, Nanoscale **10**, 10479 (2018).
[34] *Scilab, "Copyright © 1989-2005. INRIA ENPC." and "Scilab Is a Trademark of INRIA". "Www.Scilab.Org"* (n.d.).
[35] P. Lagonotte et Y. Eichenlaub, *Réseaux Électrocinétiques et Algèbre Linéaire (Notions Fondamentales)*.
[36] L. Merle, G. Manai, A. Pham, S. Lecommandoux, P. Demont, C. Bonduelle, S. Tricard, A. Mlayah, and J. Grisolia, *Enhanced Dielectric Relaxation in Self-Organized Layers of Polypeptides Coupled to Platinum Nanoparticles: Temperature Dependence and Effect of Bias Voltage*, J. Phys. Chem. C **125**, 22643 (2021).
[37] A. Bourgine, J. Grisolia, M. Vallet, D. Benoit, Y. L. Friec, V. Caubet-Hilloutou, and A. Claverie, *On the Charge Transport Mechanisms in Ge-Rich GeSbTe Alloys*, Solid-State Electron. **172**, 107871 (2020).
[38] Stauffer, D., & Aharony, A, *Introduction To Percolation Theory: Second Edition (2nd Ed.).*, Taylor&Francis. (1992).
[39] I. W. Essam, D. S. Gaunt, and A. J. Guttmann, *Percolation Theory at the Critical Dimension*, J. Phys. Math. Gen. **11**, 1983 (1978).